Complex dynamical states in binary mixture convection with weak negative Soret coupling

Arantxa Alonso,* Oriol Batiste, Alvaro Meseguer, and Isabel Mercader
Departament de Física Aplicada, Universitat Politècnica de Catalunya, Mòdul B4, 08034 Barcelona, Spain
(Received 24 July 2006; published 27 February 2007)

Binary convection in large-aspect-ratio annular containers heated from below is studied numerically for a water-ethanol mixture. High-resolution numerical tools based on spectral methods are used to solve the hydrodynamic equations in the two-dimensional approximation. The weakly nonlinear states arising very close to the onset of convection, the strongly nonlinear bursts of amplitude that precede the small-amplitude states, and the dispersive chaotic states encountered further above onset in experiments for mixtures with a weak negative Soret coupling are analyzed in detail in extended domains of aspect ratio 80. Steady localized states surrounded either by quiescent fluid or by small-amplitude waves are also obtained, and the role they play in the dynamics is elucidated.

DOI: 10.1103/PhysRevE.75.026310 PACS number(s): 47.20.Bp, 47.20.Ky, 47.27.T−, 47.54.−r

I. INTRODUCTION

Thermal convection in a binary fluid layer heated from below is a system that exhibits a great variety of pattern-forming phenomena when driven away from equilibrium [1]. Compared to convection in a pure fluid the spatiotemporal properties of the flow patterns are more complex, due to the extra degree of freedom associated with the concentration field. In binary mixtures the temperature and concentration fields are coupled through the Soret effect. The separation ratio of the mixture S is the nondimensional parameter that describes the extent to which buoyancy is modified by the Soret effect. Of special interest is the dynamics arising in $S<0$ binary mixtures. For such mixtures, the onset of convection takes place via a subcritical Hopf bifurcation once the Rayleigh number R, which is proportional to the temperature difference across the layer, exceeds a critical value R_c. The bifurcation gives rise to oscillatory patterns. The final selected nonlinear state depends on the parameters of the mixture and can take the form of (i) extended spatially uniform traveling waves, standing waves, or steady rolls, (ii) several types of localized states, and (iii) highly irregular states, which exhibit spatiotemporal chaotic motions. Although much work has been done on this system, there are still some points that remain to be clarified. To the authors' knowledge, a study of states exhibiting a complex spatiotemporal dynamics near the onset of convection in binary mixtures by means of direct numerical simulation (DNS) of the full Navier-Stokes equations is still lacking. Concerning the localized states, while localized traveling wave convection has been studied extensively for some time, localized stationary convection in the context of binary mixtures has been obtained numerically very recently [2] (such states have been named *convectons*) and has only been reported in one experiment [3], although surrounding waves were also present in that case.

In order to achieve translation-invariant systems that can support uniform traveling waves, experiments are usually performed on long, narrow annular cells. For mixtures with negative values of the separation ratio, different behaviors have been observed depending on the actual strength of S. A series of experiments using mixtures with separation ratio of around $S=-0.02$ and cells of aspect ratio of about 80 [3–5] show that, as the stress parameter $\varepsilon=(R-R_c)/R_c$ is increased through a narrow range of supercritical values ($\varepsilon\leqslant 0.02$), the system evolves through a series of complex spatiotemporal states. After some linear and nonlinear onset transients in the form of unidirectional traveling wave packets, the first persistent dynamical states observed very close to the onset of convection consist of weakly nonlinear oppositely propagating waves. Further above onset, more complex dynamical states dominated by strong nonlinear dispersion are encountered. In the so-called dispersive-chaotic regime, which is characteristic of mixtures with a weak negative Soret coupling, spatially localized regions of traveling waves repetitively form and collapse in an abrupt way leading to an erratic dynamics. In addition, the system can also evolve from this erratic state into a regime in which bursts of traveling waves coexist with a region of steady convective rolls. Finally, above a certain value of the control parameter the system settles in a pattern of nonlinear spatially uniform steady rolls which fill the cell. This diversity of states arising in large-aspect-ratio annular domains for mixtures with weak negative Soret coupling will be analyzed numerically in this paper.

The traveling wave burst and collapse process dominated by strong nonlinear dispersion has also been studied experimentally in long rectangular cells of aspect ratio between 20.0 and 40.6 [6]. Again, a sequence of very different patterns is observed in the immediate vicinity of the onset ($\varepsilon\leqslant 0.03$). A small-amplitude counterpropagating wave state is followed by a blinking traveling wave state when the left-right symmetry of the pattern is broken as ε is increased. In such states the amplitude of the traveling waves becomes spatially and temporally modulated, with a periodic modulation in short containers [7,8] and characterized by a random repetitive evolution and collapse of traveling wave bursts in longer cells [6,8]. In rectangular containers the role of the lateral walls needs to be considered, since reflections of the wave trains take place on them.

With the aim of understanding the rich dynamics encountered in experimental observations, several studies have been

*Electronic address: arantxa@fa.upc.edu

devoted to modeling the observed dynamics by using amplitude equations, usually derived after symmetry considerations and multiscale analysis. In the case of binary convection, the cubic complex Ginzburg-Landau equation (CGLE), which was first applied to pattern-forming systems in [9], is derived directly from the Navier-Stokes equations and describes the convective amplification and nonlinear evolution of a traveling wave. The coefficients of this equation for some fluids typically used in experiments were computed in [10,11]. In the limit of small amplitude and very close to the onset, the linear and nonlinear behavior of unidirectional traveling wave states was accurately fitted to the predictions of the CGLE [3].

The modulations of the waves on a slow time and space scale for a Hopf bifurcation are described by two CGLEs for the complex amplitudes of the right and left traveling waves, which include a cubic cross term in both equations that takes into account the stabilizing nonlinear interaction between oppositely propagating traveling waves [12,13]. Recently [14], a nonparametric nonlinear estimation approach was followed to fit these amplitude equations to the data corresponding to the counterpropagating regime in the experiment in the annular container [3] and the coefficient of the term that describes the interaction between the two oppositely propagating waves was determined.

Another effect that numerical simulations of the Navier-Stokes equations showed to be relevant in binary convection is the influence of the convective concentration field on the buoyancy forces and, in turn, on the growth and propagation of the traveling waves (TWs) [15,16]. Riecke [17,18] derived an additional equation governing the evolution of the amplitude of a mean large-scale concentration field. This equation takes into account the slow dynamics of the concentration field caused by the small value of the Lewis number, which measures the ratio of molecular to thermal diffusion. The extended set of coupled CGLEs accounts for the slow drift velocity and the robust occurrence of localized traveling waves, and has been used in several works to model some aspects of the dynamics of such waves [19–21].

The first time that an amplitude equation was reported to exhibit dispersive chaos was in 1983 in the work of Bretherton and Spiegel [22]. They showed that the CGLE can exhibit erratic behavior in the limit of very large dispersion, and they found the decay of the pulses to be slower than exponential and generated by an effective decrease of ε induced by the large nonlinear dispersivity of the system. Kaplan *et al.* [6] noticed that the mechanism proposed by Bretherton and Spiegel could only work for the narrowest pulses, since for initially wider pulses the bursting behavior is strongly nonlinear. They generalized the model by retaining the real part of the nonlinear term in the CGLE, and showed that this term plays an important role on the formation of pulses, since it causes the high-amplitude bursting behavior, that is, the self-focusing of the pulse. In this way they could describe the main stages in the evolution of a burst (a linear exponential amplitude growth, a faster than exponential growth due to the destabilizing effect of the real nonlinear term, and a collapse caused by compression of the pulse from the sides), and showed large nonlinear dispersion to be crucial only in the collapse process. Schöpf and Kramer [23] had also analyzed analytically the CGLE, retaining the destabilizing cubic term. They obtained chaotic states and explored their existence over a wide range of values of the coefficients relevant to binary convection, and attributed the boundedness of such states to the competition between dispersion and nonlinear frequency renormalization.

As a last remark concerning the use of CGLE to model binary convection, it is worth mentioning that since convection is triggered in the system by a subcritical bifurcation higher-order nonlinear terms should be included in the CGLE model (see [24] for a review). Kolodner *et al.* [25,26] were able to stabilize states of unidirectional TWs on the unstable branch of the subcritical bifurcation and succeeded in measuring the nonlinear coefficients of the quintic CGLE. Nevertheless, the strong nonlinear dispersion causes solutions to be bounded even without a saturating quintic term, and Kaplan *et al.* [6] showed that the nature of bursting behavior in dispersive chaos is not affected by the addition of higher-order terms.

Although the CGLE models help to identify the essential mechanisms, their range of validity is limited (e.g., a limit for the applicability of small-amplitude expansions to traveling waves arising in binary fluid convection was established in the work of [27]), and they do not reproduce all the aspects of the dynamics in a quantitative way. It is therefore necessary to carry out numerical computations of the full nonlinear convection equations to have a reliable analysis. The main difficulty in simulating this system numerically using the Navier-Stokes equations is the large size of the annular containers used in experiments. Despite the simplification due to the fact that the patterns arising in narrow containers are essentially two dimensional and can be accurately described neglecting the variations along the roll axis, the large size of the containers, whose aspect ratio can be of order 80, requires a large spatial resolution to resolve the boundary layers of the concentration field.

Most of the existing numerical works consider a single pair of rolls, so they model the dynamics of spatially uniform traveling waves and stationary states. This is the case of the extensive numerical work of Barten *et al.* [28], which studies in detail the branches of traveling waves and steady states for different values of the separation ratio. The system they consider is a two-dimensional cell such that only a single wavelength fits in the domain. In this way, the authors have obtained the bifurcation diagrams of the uniform traveling waves and stationary states and have located the transition between them.

The numerical works devoted to obtaining nonuniform solutions are less abundant. On one hand, Barten and coworkers (see, for instance, [29]) developed a finite-difference code to model binary convection in an extended container. Among other works, they analyzed the dynamics of localized traveling waves and of traveling wave fronts [15,30–32]. On the other hand, spectral methods were used by Batiste *et al.* to study the dynamics in large-aspect-ratio rectangular containers [33] or to compute the Eckhaus instability of traveling waves in annular cells [34]. Nevertheless, dispersive chaotic states have not been previously obtained by DNS of the full convection equations.

The purpose of this paper is to obtain and analyze numerically the complex low-amplitude convection arising in large-

aspect-ratio narrow annular containers for mixtures with small negative Soret coupling, extending the preliminary results presented in [35]. With that aim, we use accurate numerical tools based on spectral methods that enable us to compute the arising nonlinear patterns. We wish to compare our results with experimental observations, so we take as reference parameter values those used in experiments [3,4]. Thus, we present results for an $S=-0.021$ water-ethanol mixture filling a periodic rectangular domain of aspect ratio $\Gamma=80$ heated from below. The results we obtain are representative of the rich dynamics observed in binary mixtures with $S>-0.04$ in sufficiently long cells for Rayleigh numbers slightly above the threshold of convection.

The paper is organized as follows. In the next section we describe the numerical tools we have used. In the following section we discuss the properties of the different convection regimes we have identified in our simulations: small-amplitude time-dependent states, dispersive-chaotic solutions, and stationary localized states. Finally, the conclusions of the work are presented.

II. FORMULATION OF THE PROBLEM AND NUMERICAL APPROACH

We consider Boussinesq binary-fluid convection in a narrow annular cell in the presence of a vertical gravitational field $\mathbf{g}=-g\hat{\mathbf{e}}_z$. A vertical temperature gradient is imposed by fixing a temperature difference ΔT between the horizontal plates, with the temperature at the bottom being higher than at the top. We are interested in modeling experiments in cells with cross section width of the same order as the height d and mean circumference L much larger than d. In such systems convection settles in the form of straight rolls with the axis in the radial direction, the dynamics being essentially two dimensional. Ignoring variations along the roll axes, we use a simplified geometry consisting of a two-dimensional domain $(x,z)\in[0,L]\times[0,d]$, with the aspect ratio Γ defined as $\Gamma=L/d$ much greater than 1. Although the two-dimensional (2D) approximation may not seem to be justified in the case of the narrow cells used in the experiments we aim to model, the agreement of the numerical results with the experiments supports this assumption. The finite width of the cell is expected to alter the location of the bifurcations, but not to affect the dynamics substantially. A 3D linear stability analysis of the conduction state [36] revealed differences of 13% for the critical Rayleigh number obtained with the 2D and 3D codes for a cell of width twice its height; these differences were only slightly reduced to 6% when a parabolic Poiseuille profile was assumed in the spanwise direction.

The 2D system admits the following basic conductive state with constant gradients of temperature and concentration:

$$\mathbf{u}_c=\mathbf{0}, \tag{1}$$

$$T_c=T_0-\Delta T\left(\frac{z}{d}-\frac{1}{2}\right), \tag{2}$$

$$C_c=C_0+C_0(1-C_0)S_T\Delta T\left(\frac{z}{d}-\frac{1}{2}\right), \tag{3}$$

where $\mathbf{u}=(u,w)$ is the velocity field; T and C are the fields of temperature and concentration of the denser component, respectively; T_0 and C_0 are their mean values, and S_T is the Soret coefficient.

The dynamics of the system is governed by the continuity equation, the Navier-Stokes equations, and the energy and mass conservation equations. In their nondimensional form, scaling length with the height of the layer d, time with the vertical thermal diffusion time d^2/κ, κ being the thermal diffusivity, and temperature with ΔT, the equations explicitly read

$$\boldsymbol{\nabla}\cdot\mathbf{u}=0, \tag{4}$$

$$\partial_t\mathbf{u}+(\mathbf{u}\cdot\boldsymbol{\nabla})\mathbf{u}=-\boldsymbol{\nabla}p+\sigma\nabla^2\mathbf{u}+R\sigma[(1+S)\Theta+S\eta]\hat{\mathbf{e}}_z, \tag{5}$$

$$\partial_t\Theta+(\mathbf{u}\cdot\boldsymbol{\nabla})\Theta=w+\nabla^2\Theta, \tag{6}$$

$$\partial_t\eta+(\mathbf{u}\cdot\boldsymbol{\nabla})\eta=-\nabla^2\Theta+\tau\nabla^2\eta. \tag{7}$$

Here, Θ denotes the departure of the temperature from its conduction profile, $\Theta=(T-T_c)/\Delta T$, and $\eta=-(C-C_c)/[C_0(1-C_0)S_T\Delta T]-\Theta$. The dimensionless parameters in the above equations are the Rayleigh number R, the Prandtl number σ, the Lewis number τ, and the separation ratio S, defined as

$$R=\frac{\alpha\Delta T g d^3}{\kappa\nu},\quad \sigma=\frac{\nu}{\kappa},\quad \tau=\frac{D}{\kappa},\quad S=C_0(1-C_0)\frac{\beta}{\alpha}S_T,$$

where α and β are the thermal and concentration expansion coefficients, ν is the kinematic viscosity, and D is the mass diffusivity.

The boundary conditions are taken to be periodic in x with period Γ. No slip, fixed temperature, and no mass flux at the top and bottom plates are considered

$$\mathbf{u}=\Theta=\partial_z\eta=0\quad \text{on } z=0,1. \tag{8}$$

As a measure of the heat transport by convection, we use the Nusselt number Nu, defined as the ratio of heat flux through the top plate to that of the corresponding conductive solution. It has the following expression:

$$\mathrm{Nu}=1-\Gamma^{-1}\int_{x=0}^{x=\Gamma}\partial_z\Theta(z=1)dx.$$

Most of the calculations carried out in this paper are aimed at obtaining time-dependent solutions and they have been computed with a time-evolution code. To integrate the equations in time, we have used the second-order time-splitting algorithm proposed in [37], combined with a pseudospectral discretization in space (Galerkin Fourier in x and Chebyshev-collocation in z). The Helmholtz and the Poisson equations resulting from the time splitting are solved by using a diagonalization technique [38]. The authors have successfully used this algorithm previously to study binary convection in large-aspect-ratio rectangular containers [33].

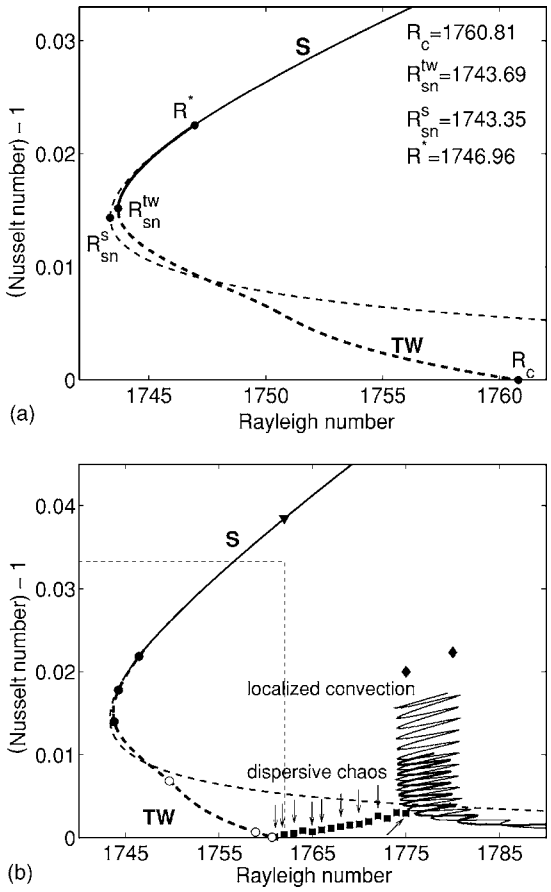

FIG. 1. (a) Bifurcation diagram (Nu −1 versus Rayleigh number) showing the stationary (S) and traveling wave (TW) branches of solutions of wave number $k=\pi$ for an $S=-0.021, \sigma=6.22, \tau=0.009$ binary mixture. The critical Rayleigh numbers at the onset of convection R_c, at the saddle-node bifurcations in the TW branch R_{sn}^{tw} and in the stationary branch R_{sn}^{s}, and at the parity-breaking bifurcation of the stationary solutions where the traveling waves disappear R^* are indicated in the plot. (b) Bifurcation diagram including the subharmonic instabilities in the TW branch (the open and solid circles indicate loss and gain of stability, respectively, in the subharmonic bifurcations), the region where dispersive chaotic states are observed (solid squares), and the region of localized convection (two odd and even parity snaking branches of steady localized convection). The straight dashed lines delimit the part of the bifurcation diagram depicted in (a), the arrows indicate the small-amplitude and dispersive chaotic states shown in the paper, the solid triangle corresponds to the stationary state reached in Fig. 3, and the solid diamonds show the location of the two localized states depicted in Fig. 10.

In addition, to calculate the steady solutions and the spatially uniform traveling waves, both stable and unstable, in an efficient way we have adapted a pseudospectral first-order time-stepping formulation to apply Newton's method [39,40]. Finally, it is also possible to carry out an Eckhaus stability analysis of these solutions using Floquet theory, as we presented in a previous work [34]. We include in Fig. 1 the bifurcations that were identified in the branch of traveling waves for the mixture we are studying in the present paper.

III. RESULTS

In this section we discuss the dynamics arising in a water-ethanol mixture with parameters $S=-0.021$, $\sigma=6.22$, and $\tau=0.009$ filling a periodic container of horizontal aspect ratio $\Gamma=80$ when a vertical temperature gradient is applied. This choice of parameters is motivated by the experiment of Kolodner *et al.* [4]. For most of the computations done with the time-evolution code we have used 32 collocation points in the vertical direction z, 1000 points for the Fourier pseudospectral evaluation in the horizontal direction x, and a time step $\Delta t=10^{-3}$ in units of the vertical thermal diffusion time. We have checked the validity of the resolution we were using by increasing the horizontal resolution to 2000 for some solutions.

A. Bifurcation properties of spatially uniform solutions

In large-aspect-ratio annular containers, spatially uniform solutions in the form of traveling waves and stationary convection can be selected by the system. These solutions consist of pairs of rolls with their axis oriented perpendicular to the long sidewalls. The number of pairs of rolls of the structure adapts itself to the size of the container, and for the $\Gamma=80$ cell we are considering, the critical wave number of the solutions is $k=\pi$, giving rise to solutions formed by $n=40$ pairs of rolls. The bifurcation diagram in Fig. 1(a) shows the branches of spatially uniform solutions for an $S=-0.021$ mixture computed with $k=\pi$. For sufficiently negative values of the separation ratio, the primary instability of the conduction state is oscillatory. This instability gives rise to a branch of traveling waves that bifurcates subcritically from the conduction state for $R_c=1760.81$. These TWs, which can travel either to the right or to the left, are unstable at the onset of convection and typically acquire stability in a secondary saddle-node bifurcation located at $R_{sn}^{tw}=1743.69$. When the Rayleigh number is increased from the saddle-node point, the TW branch disappears for $R^*=1746.96$ in a parity-breaking bifurcation of steady solutions, to which stability is transferred. The phase velocity of the TW decreases monotonically from its Hopf value at the onset of convection R_c to zero at the bifurcation point that gives rise to the stable stationary states R^*. As can be seen in the diagram, there is also a saddle-node bifurcation point in the branch of stationary solutions, which is located at $R_{sn}^{s}=1743.35$.

Sideband instabilities (instabilities that modify the spatial periodicity of the basic solution) are known to play an important role in large-aspect-ratio containers. To find out whether the bifurcation diagram in Fig. 1(a) is modified or not when Eckhaus instabilities are considered, we analyzed in a previous work the stability of the traveling waves with respect to subharmonic disturbances [34,35]. The Eckhaus bifurcations that were identified are depicted in the TW branch in Fig. 1(b). The first Eckhaus instability occurs nearly at the critical point, and is followed by two additional destabilizing bifurcations (open circles). As can be seen in the figure, the subsequent stabilizing Eckhaus bifurcations (solid circles) take place in the upper part of the TW branch, which means that the uniform TW solution does not gain stability at the saddle-node point. Indeed, the last stabilizing

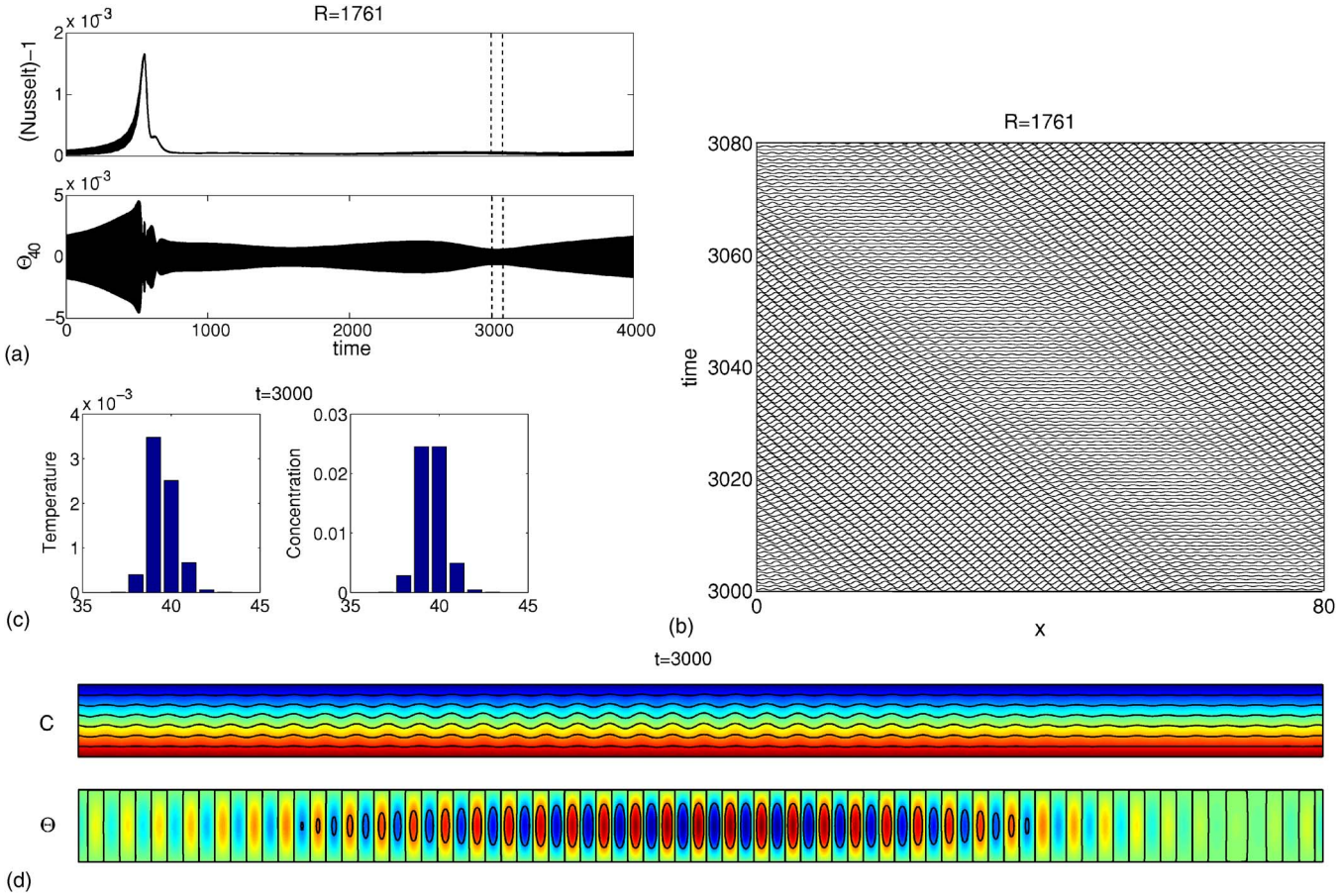

FIG. 2. (Color online) $R=1761$ ($\varepsilon=0.108\times10^{-3}$). (a) Time series (Nusselt number and $n=40$ Fourier mode of temperature versus time), (b) space-time plot of midplane temperature, (c) bar charts showing the Fourier spectra in the x direction of temperature and concentration for the solution at $t=3000$, and (d) contour plots of the concentration and temperature fields at the same time-instant (while Θ shows deviations from temperature in the conduction state, C always includes the linear concentration profile). The space-time plot shows the small-amplitude modulated TW that forms after the initial burst of amplitude; the modulation travels in the same direction as the TW. The time interval of the space-time plot is indicated on the time-series diagram with vertical dashed lines.

Eckhaus bifurcation takes place very close to the region of transition from traveling wave to steady convection, causing the region of stability of the traveling waves to be extremely small.

The bifurcation diagram in Fig. 1(b) also includes the region where stable dispersive-chaotic states (solid squares) and localized states are encountered. For the small-amplitude time-dependent solutions the Nusselt number has been averaged in time. The two intertwined snaking branches of localized solutions, computed with the continuation code, correspond to odd and even parity stationary solutions. The stability of the these branches has not been analyzed, so in this case the use of solid lines does not indicate that solutions are stable all along the branches. Both the time-dependent states and the localized stationary states will be discussed in detail in the following sections. For Rayleigh numbers above $R\approx1785$ the system always evolves to the spatially extended stationary nonlinear solution.

B. Low-amplitude time-dependent states

For slightly supercritical Rayleigh numbers, a convective regime, completely different from the spatially uniform TW and stationary solutions, but consistent with experimental observations, is identified for mixtures with a separation ratio value close to zero. Our simulations show that, depending on the initial conditions, the system remains in long-lived very small-amplitude states instead of making a transition to a large-amplitude stable state, a uniform $n=40$ stationary state in the case of an $S=-0.021$ mixture in a $\Gamma=80$ container. Such small-amplitude states are never observed for subcritical values of the Rayleigh number ($R<R_c$).

The first regime we obtain, extremely close to the onset of convection and starting our simulations from small noise, is a state of unidirectional modulated traveling waves, which is preceded by a burst of convection amplitude. The structure of this state can be visualized in Fig. 2 for $R=1761$ ($\varepsilon=0.108\times10^{-3}$). The figure includes two time series showing the evolution of the Nusselt number and the $n=40$ temperature mode, the space-time plot showing the variation with time of temperature in the midplane of the cell, the temperature and concentration bar charts showing the contribution of each Fourier mode to the solution at $t=3000$, and the contour plots of the temperature and concentration fields also at $t=3000$. The system remains a long time in a very small-

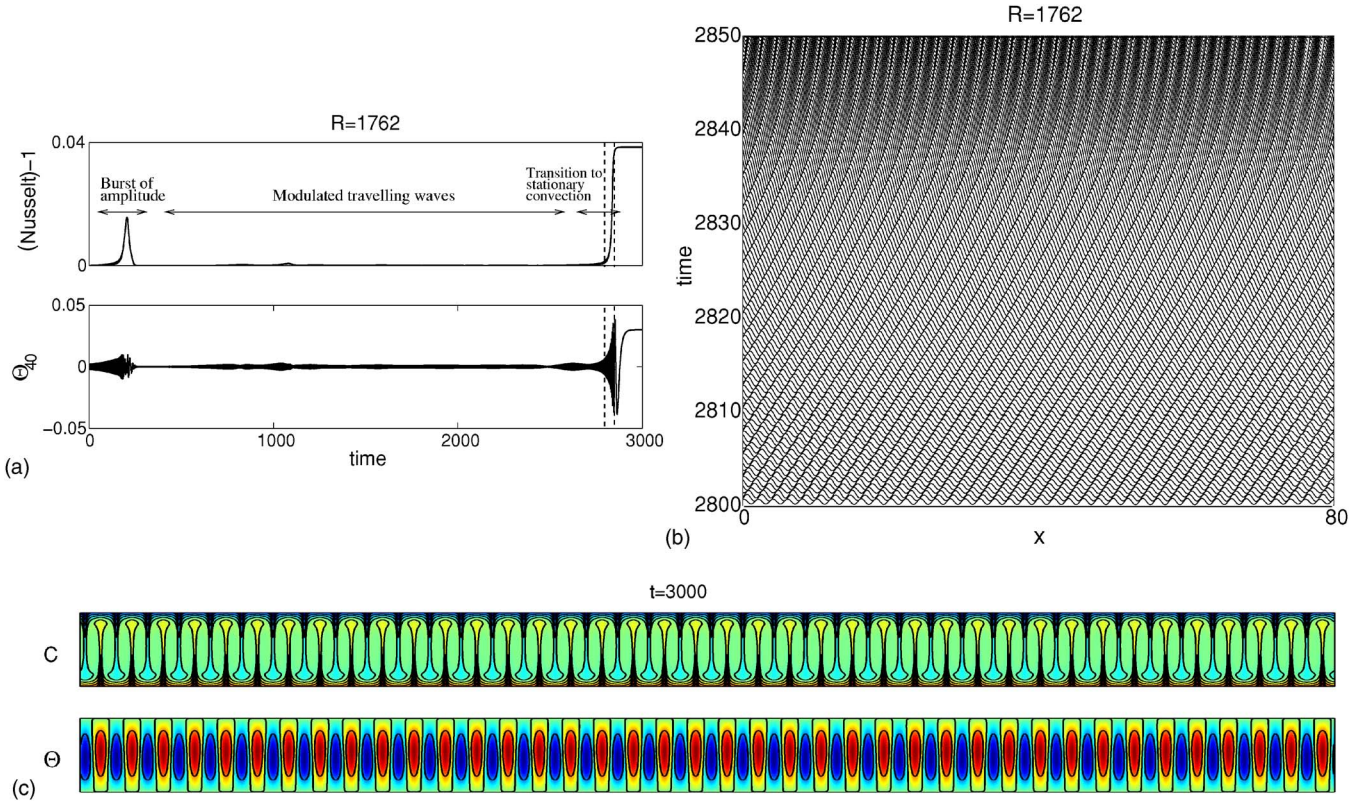

FIG. 3. (Color online) $R=1762$ ($\varepsilon=0.676\times10^{-3}$). (a) Time series (Nusselt number and $n=40$ Fourier mode of temperature versus time), (b) space-time plot of midplane temperature, and (c) contour plots of the concentration and temperature fields for the solution at $t=3000$. Three stages can be distinguished in the evolution of the system: an initial burst of convection amplitude, a regime of unidirectional modulated traveling waves, and a transition to stable uniform stationary convection. The space-time plot shows the transition to stationary convection.

amplitude state consisting of a slightly modulated left-traveling wave in which the modulation travels in the same direction as the traveling wave and at about the same velocity, as can be appreciated in the space-time plot. The spatial Fourier spectrum of the solution a $t=3000$ shows that the contribution of the $n=39$ Fourier mode at this early stage of convection is of the same importance as that of the critical $n=40$ mode, and that the contribution of the $n=38$ and 41 Fourier modes is also relevant. Since we are very close to the onset of convection, we can estimate the phase and group velocity from the linear stability analysis of the conduction state [36]. We obtain the following critical Rayleigh numbers and frequencies for the $n=39,40,41$ traveling waves ($k_{39}=3.0631$, $k_{40}=3.1416$, $k_{41}=3.2201$): $R_{39}=1761.48$, $R_{40}=1760.82$, $R_{41}=1763.32$ and $\omega_{39}=2.7413$, $\omega_{40}=2.8084$, $\omega_{41}=2.8771$. The resulting phase and group velocity turn out to be very similar, $c_p^{40}=\omega/k=0.89$ and $c_g\approx\Delta\omega/\Delta k=0.86$, in agreement with the space-time plot.

However, this weakly nonlinear state turns out to be unstable. The amplitude of the unidirectional traveling wave grows superexponentially and the system undergoes a transition to the fully nonlinear spatially uniform stationary solution with azimuthal wave number $n=40$. We can observe this behavior in Fig. 3 (in this case the small-amplitude TW travels in the opposite direction), for a slightly superior value of the control parameter, $R=1762$ ($\varepsilon=0.676\times10^{-3}$). Again, simulations show that a burst of convection amplitude precedes the regime of weakly modulated traveling waves. The linear growth in the beginning gives rise to a burst of amplitude, and the subsequent collapse leaves the system in the small-amplitude unidirectional right travelling wave state. In real time, for the parameters of the fluid used in [3], the system remains in such state for about 40 h before evolving to the large-amplitude stationary state.

The next dynamical regime attained by the system when increasing further the Rayleigh number and taking as initial condition for the simulation the small-amplitude modulated TW state for $R=1762$ is the so-called *counterpropagating regime* [3]. This state is represented in Fig. 4 for $R=1763$ ($\varepsilon=1.24\times10^{-3}$) and consists of two asymmetric wave packets propagating in opposite directions along the cell. The temperature and concentration bar-charts of the solution at $t=15\,000$ reveal an important contribution of the Fourier modes in the range $37\leqslant n\leqslant42$. The system persists in this state; the duration of the time series shown in Fig. 4 is extremely long, corresponding to about 250 h for the parameters used in [3], and a transition to the stationary state has not been observed. The stabilizing effect of the nonlinear interaction between oppositely propagating traveling waves is a well-known property that can be modeled by writing two CGL equations for the amplitudes of the right and left traveling waves [13]. In agreement with experimental observations, the amplitude of convection remains very small.

Remarkably, as in the previous cases, we can appreciate in the time series of Fig. 4 that the system exhibits two bursts of

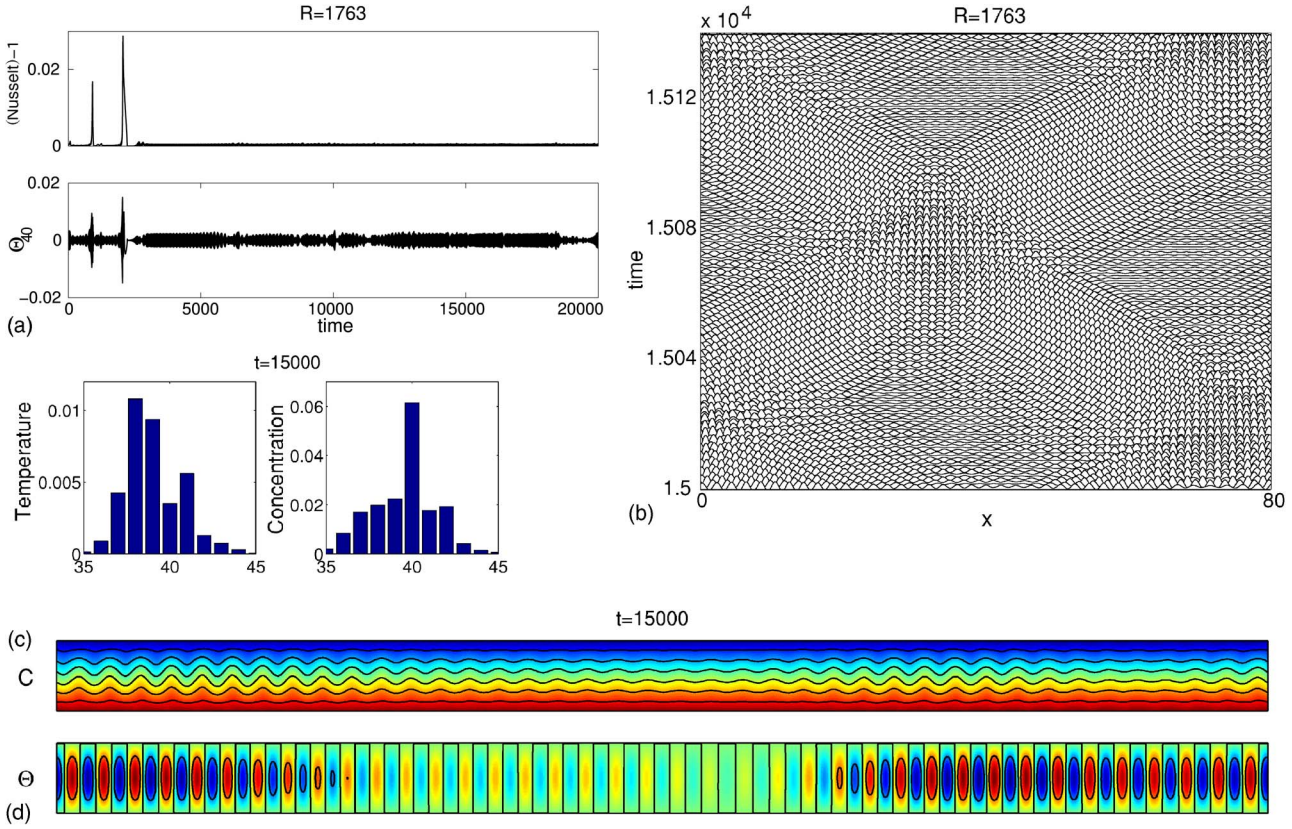

FIG. 4. (Color online) $R=1763$ ($\varepsilon=1.24\times10^{-3}$). (a) Time series (Nusselt number and $n=40$ Fourier mode of temperature versus time), (b) space-time plot of midplane temperature, (c) bar charts showing the Fourier spectra in the x direction of temperature and concentration for the solution at $t=15\,000$, and (d) contour plots of the concentration and temperature fields at the same time instant. After the two initial bursts of convection amplitude the system settles in a small-amplitude *counterpropagating* regime; the interaction between the wave packets traveling in opposite directions has a stabilizing effect on the system.

convection amplitude before the counterpropagating regime sets in. An abrupt increase in the amplitude of convection takes place in the system, which is followed by a sudden collapse of convection.

To elucidate what happens during the bursting episodes, it is worth analyzing in detail the spatiotemporal nature of the solution during the bursts. To that end, we have included in Fig. 5 and Fig. 6 the space-time diagram, the contour plots of the concentration field in several time instants, and the corresponding time series in two cases: the burst of amplitude observed for $R=1762$ and the second burst that takes place for $R=1763$. The dynamics in both processes is quite spectacular and, as will be shown, the developing patterns clearly depart from a weakly nonlinear regime at some stages of the evolution.

We begin by discussing the evolution of the system during the burst of amplitude observed for $R=1762$, which can be visualized in Fig. 5. At the beginning of the process, prior to the burst of amplitude, a fast left traveling, nearly uniform wave of small amplitude and wave number $n=40$ develops (contour plot for $t=150$). As the amplitude of the wave grows the traveling wave slows down, but this growth does not take place homogeneously throughout the cell. At $t\approx195$, spatial nonuniformities in the solution can be clearly appreciated in the contour plots of the concentration field, and approximately at this time instant a spatiotemporal defect located at $x\approx60$ can be observed in the space-time plot of temperature in Fig. 5(b). On the right hand side of the defect, a spatially localized fast traveling pulse, which keeps its amplitude constant, develops. On its left hand side, the amplitude of convection begins to grow significantly and, as the wave slows down, the large-amplitude convective region progressively becomes confined in space. In addition, the fast traveling pulse collides with it, and an abrupt collapse of the structure takes place ($t=220-230$). The region of finite-amplitude convection shrinks very fast and is replaced by totally quiescent fluid ($t=230$). The system is left in a slightly perturbed conduction state at the end of the process ($t=280$).

The spatiotemporal evolution of the pattern during the second burst that takes place for $R=1763$ can be seen in Fig. 6. Analogously to the previous case, a small-amplitude fast $n=40$ left traveling wave begins to grow in the system triggered by the oscillatory instability. This time the growth appears to be quite uniform and the dynamics one might expect beforehand, after an inspection of this early stage of the evolution of the pattern (until $t\approx2040$), would be a faster than exponential growth bringing the system to the stable uniform stationary solution, similar to that represented in Fig. 3 for $R=1762$. Instead, spatial inhomogeneities develop again in the pattern. The space-time plot of temperature reveals a defect located in $x\approx50$ at $t\approx2060$, which separates a small-

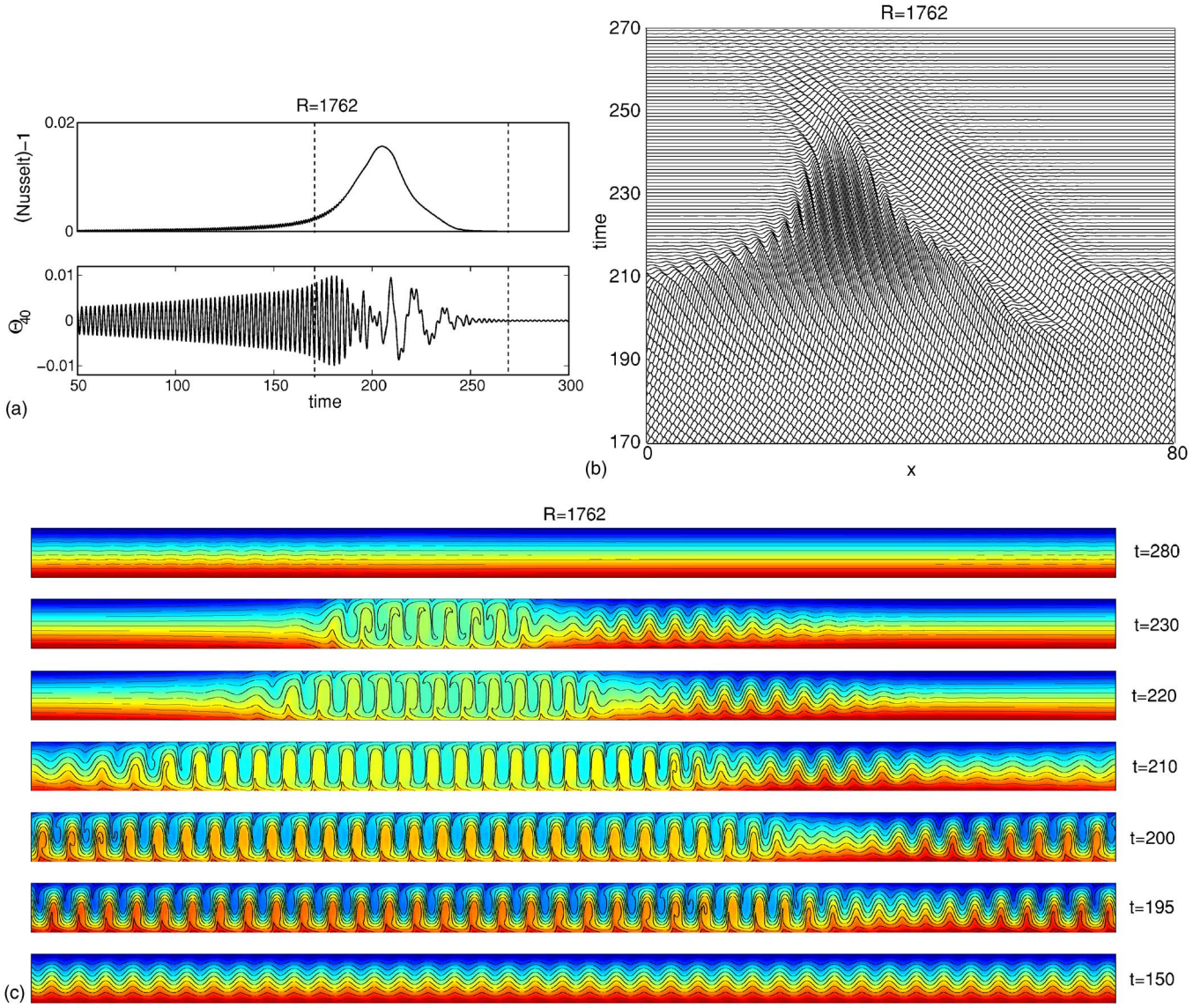

FIG. 5. (Color online) (a) Time series (Nusselt number and $n=40$ Fourier mode of temperature versus time), (b) space-time plot of midplane temperature, and (c) contour plots of the concentration field in different time instants during the burst of amplitude for $R=1762$.

amplitude fast traveling pulse from a region of large-amplitude slowly traveling convection. In this case, though, the spatial extension of the pulse is very small and it is damped very fast, leaving a void in the structure that expands in both directions by slowly eroding the nearly stationary large-amplitude structure. After the disappearance of the pulse, the system is left in a state in which large-amplitude stationary convection coexists with quiescent fluid. Such states of localized steady convection resemble the stable states that will be presented later. Since for the Rayleigh number we are considering we are outside the region of existence of these states, the convection region gradually reduces its size and is replaced with totally quiescent fluid. The system ends up in an almost conductive state from which the counterpropagating regime will emerge.

Our results should be contrasted with the mechanisms proposed by Kaplan *et al.* [6] for the spatiotemporal evolution of bursts of amplitude. Kaplan *et al.* distinguish between initially wide and narrow pulses, and they propose two different mechanisms depending on the initial width of the burst.

We believe that the spatiotemporal behavior during the pulse depicted in Fig. 5 for the burst for $R=1762$ may follow the nonlinear *self-focusing* mechanism they propose for initially wide pulses. They divide the evolution of these pulses into three stages: a linear exponential amplitude growth, a faster than exponential growth, and the collapse. During the linear growth the pulse amplitude increases exponentially, while during the nonlinear stage the amplitude growth is followed by a fast narrowing of the pulse. The collapse is initiated as a compression of the pulse at the edges, and when the pulse becomes narrow enough the decay to small amplitude takes place very rapidly, in what they call a self-focusing scenario. According to them, the cubic CGLE can account for this behavior, provided the real part of the nonlinear term is not neglected, since bursting occurs due to its

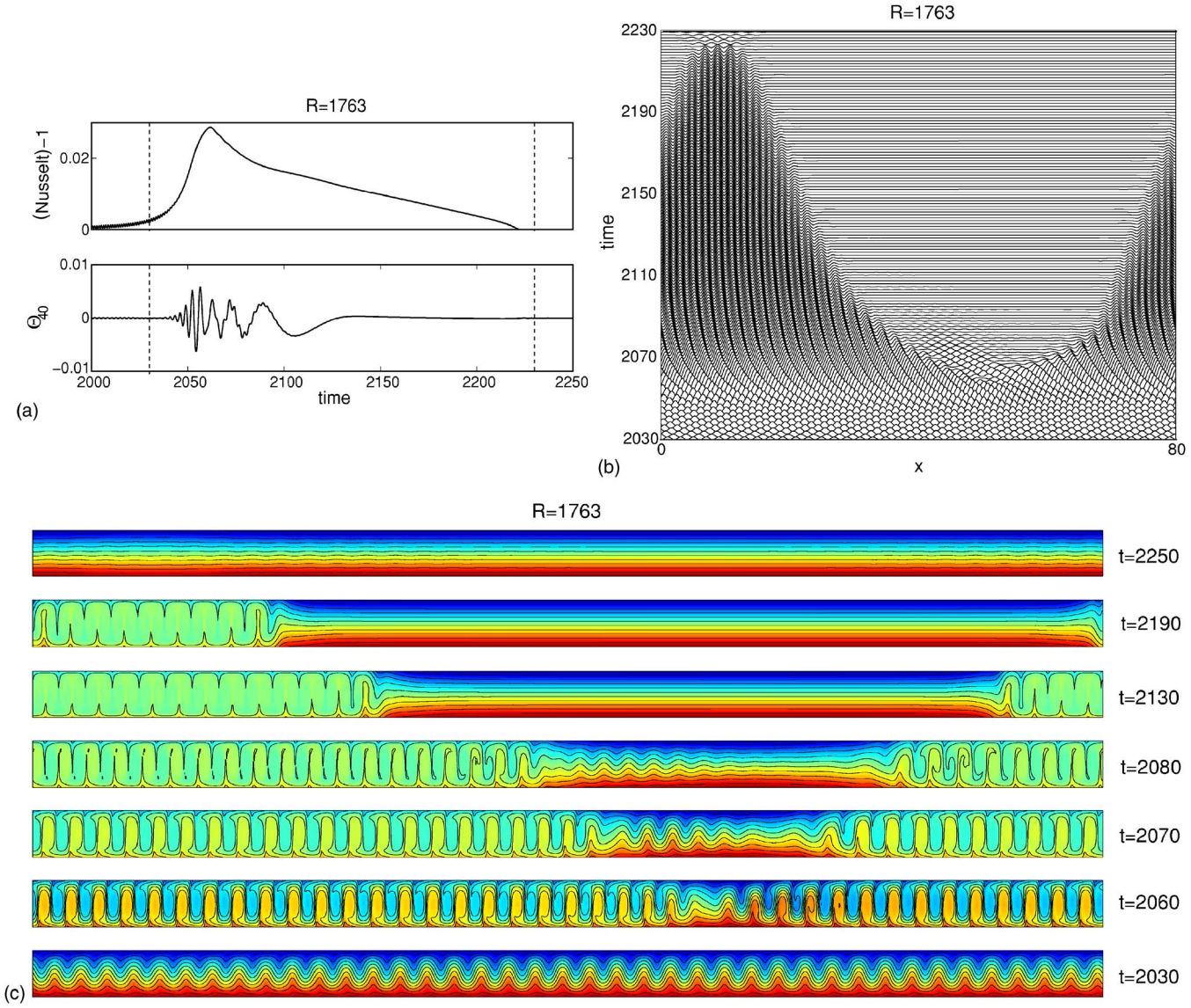

FIG. 6. (Color online) (a) Time series (Nusselt number and $n=40$ Fourier mode of temperature versus time), (b) space-time plot of midplane temperature, and (c) contour plots of the concentration field in different time instants during the burst of amplitude for $R=1763$.

destabilizing role, which is responsible for the faster than exponential growth and leads to the formation of a singularity in a finite time. Initially the pulse is quite uniform; as the pulse evolves the largest amplitude gradients take place near the pulse edges and produce wave number variations, while the amplitude inside the pulse continues to grow faster than exponentially. This produces the self-focusing of the pulse and the collapse occurs due to compression of the pulse caused by the strong nonlinear dispersion of the system.

In contrast, we think that the collapse process depicted in Fig. 6 for the second burst taking place for $R=1763$ differs from the mechanisms proposed in [6]. Instead of a fast collapse of the pattern, the system reaches a localized stationary state of a large number of rolls, eventually decaying to conduction by the gradual loss of all the pairs of rolls that make up the pattern. Nonlinear dispersion is not relevant in the destruction of convection; thus, neither the Bretherton-Spiegel mechanism [22] nor the self-focusing mechanism proposed by Kaplan *et al.* would be suitable for the description of this collapse process. In addition, it is worth emphasizing that previous works always talk about pulses of traveling waves, while our simulation shows that in this case the system reaches a state in which a pair of moving fronts separates uniform steady convection from the conductive state. Such states are reminiscent of the stable localized steady states discovered in [2].

C. Dispersive chaotic states

A slight increase in the Rayleigh number produces a transition from the counterpropagating regime to the dispersive chaos regime. In Fig. 7 we have included several time series showing the variation of the Nusselt number [Fig. 7(a)] and the $n=40$ temperature mode [Fig. 7(b)] for several values of the Rayleigh number in the range $1765 \leqslant R \leqslant 1775$ ($2.38\times10^{-3} \leqslant \varepsilon \leqslant 8.01\times10^{-3}$), during the dispersive chaos

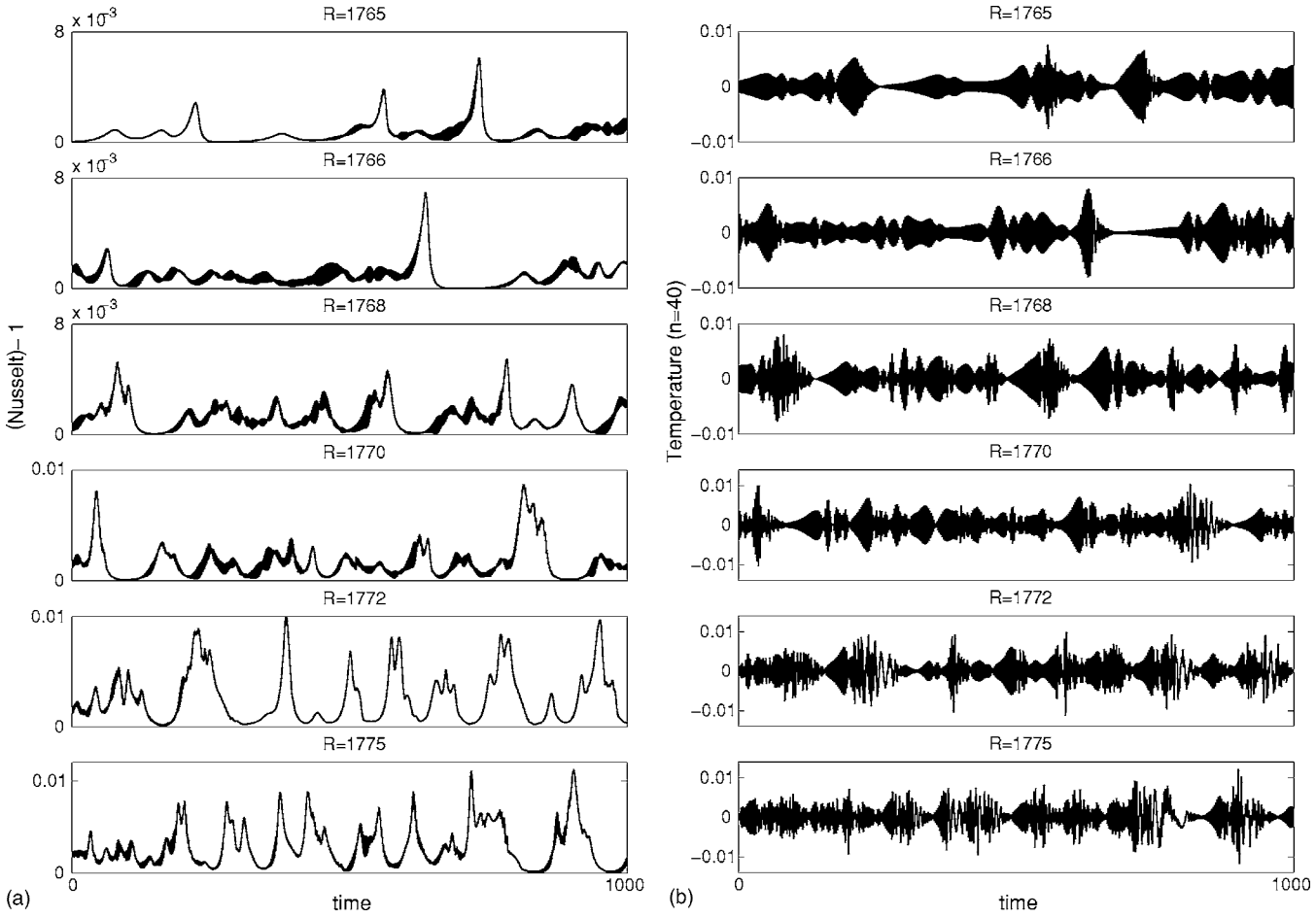

FIG. 7. Temporal series showing the variation of (a) the Nusselt number and (b) the $n=40$ temperature mode in one point (right) for different values of the Rayleigh number during the dispersive chaotic regime.

regime. These states have been obtained sequentially starting the simulations from the previous dispersive chaotic state (that is, the state obtained with the preceding Rayleigh number). As can be appreciated in the plot, the dynamics becomes erratic. The Nusselt number, which is a global variable that gives an indication of the strength of convection in the whole annulus, oscillates aperiodically. We observe that the amplitude of convection of these states remains small until quite suddenly a burst of convection amplitude takes place in the system. This sequence of small-amplitude convection followed by a burst and the subsequent collapse of amplitude repeats irregularly. The frequency and intensity of these bursts changes in each episode, and these two magnitudes increase as the Rayleigh number is increased. Whereas for $R=1765$ only three relatively small-amplitude bursts are recorded during the time interval $0<t<1000$, roughly ten larger-amplitude bursts take place in the system for $R=1775$ during the same time interval. The intensity of the bursts for $1770<R<1775$ typically reaches a value of $\mathrm{Nu}\approx 0.01$, which represents approximately 25% of the Nusselt number corresponding to the spatially uniform steady solution (see bifurcation diagram in Fig. 1).

To visualize the spatiotemporal features of these chaotic states, we include in Fig. 8 the space-time plots of temperature and the contour plots of concentration at $t=1000$ for three values of the Rayleigh number during the dispersive chaos regime: $R=1769$, 1772, and 1775. Spatially localized traveling pulses of convection, of different length and duration, grow and decay around the cell. Regions of the cell with large convection amplitude coexist with areas of nearly quiescent fluid. This behavior can be observed, for instance, for $R=1769$ at $t=1000$. The contour plots show the formation of a highly localized pulse on the left-hand side of the cell, while on the right-hand side a region without convection develops. Such quiescent regions can also be observed in the simulations for $R=1769$ in the range $1100<t<1140$ on the right-hand side of the container, and for $R=1772$ in the range $1080<t<1120$. Broader pulses can be observed, for instance, for $R=1775$. As the Rayleigh number increases, the variations of the structure in time are more rapid and the dynamics becomes more erratic; the pulses appear more densely in space. In addition, for high values of the control parameter ε, the pulses tend to appear at similar spatial locations, as happens for $R=1775$. This memory effect is due to the combined facts that, on one hand, a large value of ε encourages the formation of pulses, and, on the other, the time scale for the diffusion of concentration is large as a result of the small Lewis number of the mixture.

We have also explored the influence of the size of the container on the dynamics. Simulations of convection in a

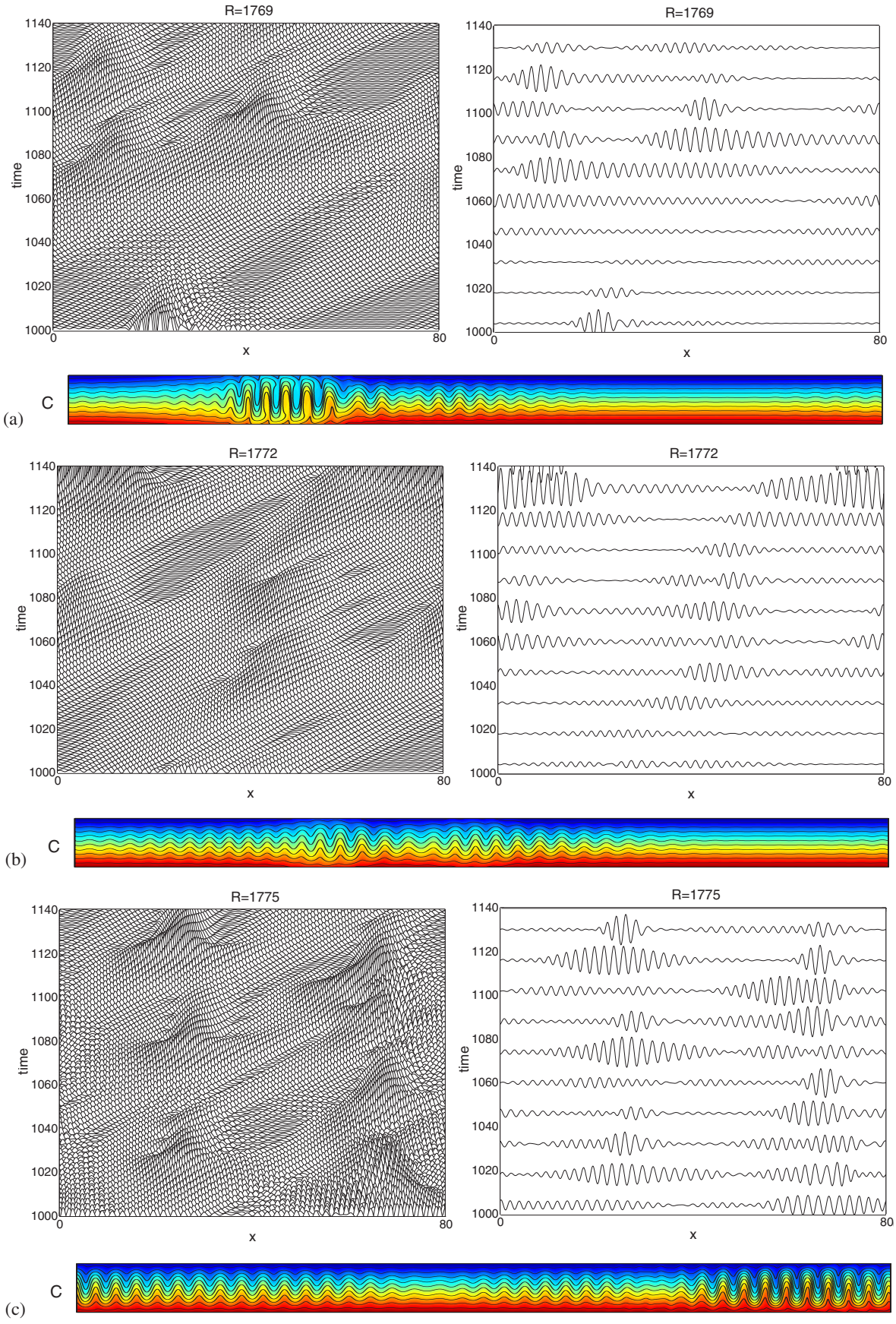

FIG. 8. (Color online) Space-time plots of midplane temperature and concentration contour plots of the solution at a $t=1000$ for three values of the Rayleigh number during the dispersive chaotic regime: $R=$(a) 1769, (b) 1772, and (c) 1775.

container of aspect ratio $\Gamma=60$ for the same binary mixture reveal a dynamics analogous to that of the $\Gamma=80$ cell. The dispersive chaos regime is thus observed in smaller aspect ratio containers and shares the same features. Nonchaotic small-amplitude states similar to those described previously are also observed before the chaotic regime sets in, although for the $\Gamma=60$ cell we have been able to obtain much more regular, nearly periodic, and quasiperiodic states. Finally, it should be mentioned that in the case of a $\Gamma=40$ container the system did not reach the chaotic regime. For the trials we have made using slightly supercritical Rayleigh numbers and different initial conditions, the selected solution was always the spatially uniform fully nonlinear stationary state. However, since we have not explored the parameter space exhaustively, we cannot totally exclude the possibility that the system remains in small-amplitude states, although for the $\Gamma=80$ and 60 cells such states were reached very easily in the simulations.

Our numerical results on the dispersive chaos regime agree with the experimental observations in annular containers [3–5]. In addition, we have confirmed that the origin of this regime is large nonlinear dispersion by doing some simulations with smaller values of the separation ratio of the mixture, $S=-0.041,-0.061,-0.081,-0.101,-0.121$, since making S more negative is known to reduce nonlinear dispersion [5]. Taking as initial condition of the simulations the chaotic solution for $R=1770$, and keeping constant the control parameter to a value of $\varepsilon=5\times10^{-3}$ (for each value of S we have computed the critical Rayleigh number with a linear stability code), we observe a trend in the bursts to decrease progressively in frequency and amplitude. At $S=-0.101$ a dispersive chaotic state no longer persists and the system selects a localized TW state.

We believe that the original mechanism proposed by Bretherton and Spiegel [22] and confirmed by Kaplan *et al.* [6] to describe the evolution of narrower pulses applies in these numerical observations. In this mechanism, the growth of these pulses is linear, so they follow a slower than exponential growth, the decay is generated by the renormalization of ε due to the wavenumber variations, and the pulse is destroyed before it can grow significantly. This scenario is reproduced by neglecting the real part of the nonlinear term in the CGLE and nonlinear dispersion is relevant during the whole evolution of the pulse.

D. Localized convection

The dispersive chaos regime we have described in the previous section is persistent; the system can remain indefinitely in such states. As we have seen in the space-time plots, after most of the bursts of amplitude, the system goes back to a small-amplitude state. Nevertheless, in some occasions our simulations show that the system makes a transition to a large-amplitude nontraveling localized state, whose length can vary. Depending on the Rayleigh number and the initial conditions, the system will follow one of several paths. Either it will remain in this localized state, or it will return to the dispersive chaos state, or it will evolve to the spatially uniform steady solution. For instance, the space-time plot for

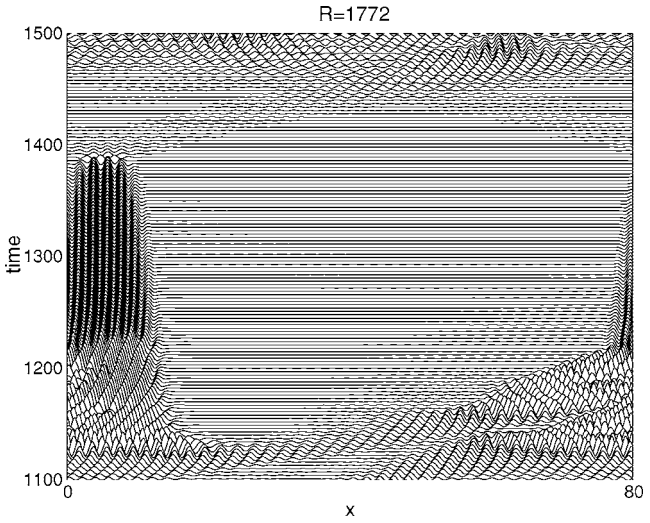

FIG. 9. Space-time plots of midplane temperature for $R=1772$ showing the formation of a stationary localized state out of the dispersive chaotic state and its subsequent destruction bringing the system back into the chaotic regime.

$R=1772$ included in Fig. 9, obtained by extending the simulations of Fig. 8(b), shows the formation of a localized stationary structure out of the dispersive chaos regime and its subsequent destruction.

The stable nontraveling localized states we have obtained are represented in Fig. 10. Such states consist of a localized region of large amplitude steady convection, which is either surrounded by quiescent fluid [Fig. 10(a)] or embedded in a background of small-amplitude waves [Fig. 10(b)]. In experiments, only the stationary localized states sustained by waves have been observed [3].

The localized state represented in Fig. 10(b) for $R=1780$ has emerged directly from a dispersive chaotic state and resembles the localized states observed in the experimental work of [3]. The authors of [3] refer to these states as the *coexistence regime*, since they observe regions occupied by almost perfectly steady rolls surrounded by TWs whose amplitude varies regularly in time. Nevertheless, while the amplitude of the waves remains small in our simulations, it reaches large values in the experimental observations.

The stationary localized state included in Fig. 10(a) for $R=1775$ has been obtained by considering as initial solution for the simulations the time-dependent localized state for $R=1780$ and reducing the Rayleigh number progressively. The length of the convection region is exactly the same as in the solution for $R=1780$, but now the rest of the fluid is in a perfect conducting state despite the uniform heating from below. Such states have been obtained for the first time in binary mixtures by Batiste and Knobloch in a very recent numerical work considering ^{3}He-^{4}He mixtures (mixtures with a large negative Soret coupling) [2], and have been named *convectons*. In our simulations, we find that the convectons can be stable in the following range of Rayleigh numbers: $1774\leqslant R\leqslant1779$. Below $R=1774$, the two fronts that separate the steady convection region from the conduction part unpin and the convecton is destroyed by the progressive suppression of pairs of rolls; the system returns to

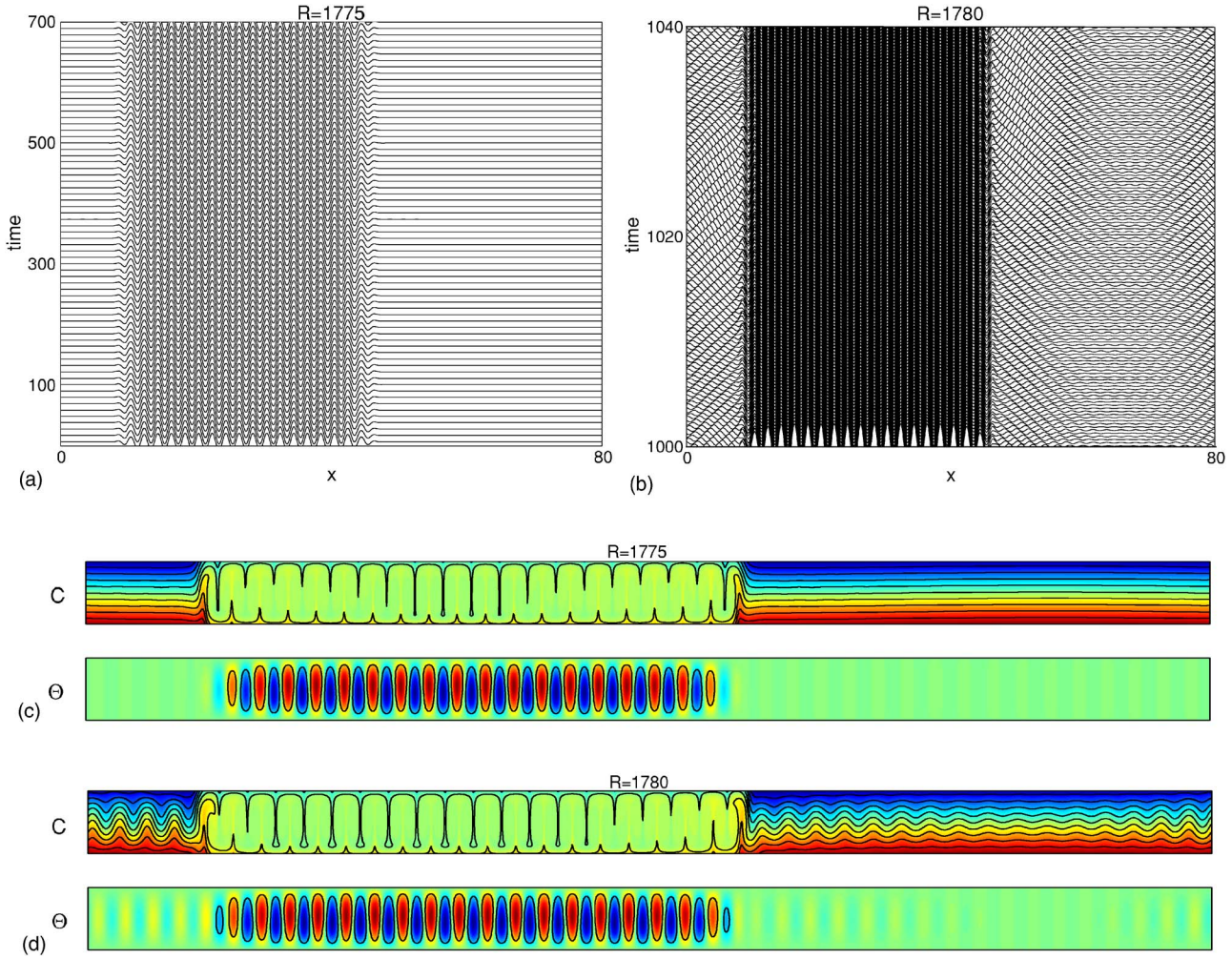

FIG. 10. (Color online) Space-time plots of midplane temperature for (a) a stationary localized state (convecton) for $R=1775$ and (b) a stationary localized state coexisting with small-amplitude waves for $R=1780$. The corresponding temperature and concentration contour plots are depicted in (c) and (d).

the dispersive chaos state from which a new convecton may arise. This process is illustrated in Fig. 11(a) for $R=1771$. Above $R=1779$ the fronts begin to move apart until the cell is filled with spatially uniform stationary convection, as can be seen in Fig. 11(b) for $R=1780$. It is worth noticing that the stationary convecton is no longer stable for $R=1780$ [Fig. 11(b)], but it can remain stable provided waves appear in the conduction region [Fig. 10(b)]. Therefore, these surrounding waves have a stabilizing effect on the localized structure by colliding with the convecton. We have been able to find convectons stabilized by waves up to $R=1784$; for Rayleigh numbers above $R\approx 1785$ stable localized states are not found any more, and convection is always in the form of uniform steady rolls.

A striking feature of the convectons is the arbitrariness of their length. For a fixed value of the Rayleigh number there is multiplicity of stable localized states, each formed by a different number of convection rolls. A theoretical interpretation of this behavior has been proposed recently by Burke and Knobloch [41] in the context of the Swift-Hohenberg equation. They obtain branches of solutions for the convectons that "snake" from the conduction state to the spatially uniform stationary state. We have been able to compute these snaking branches using the full Navier-Stokes equations, and have included them in the bifurcation diagram in Fig. 1(b). Each of the curves corresponds to convectons of either odd or even parity. In each right turning point the convecton acquires a pair of rolls; thus, the length of the convecton increases progressively and approaches the spatially uniform solution. The number of rolls of the localized solution in the piece of odd branch shown in the plot (the shorter one), varies from eight single rolls below the first saddle node to 20 after the last saddle node. In the piece of even branch shown, the number of single rolls lies between seven and 31. These snaking branches are independent of the value of the aspect ratio of the cell in the region shown; the only variation would be the actual value of the Nusselt number, which would be scaled by a factor since its definition includes an average over the horizontal size of the container. However, the snaking branches connect the conduction state with the spatially uniform stationary state, which is formed by a different number of rolls for each value of Γ, so the number of turning points must depend on the aspect ratio of the cell,

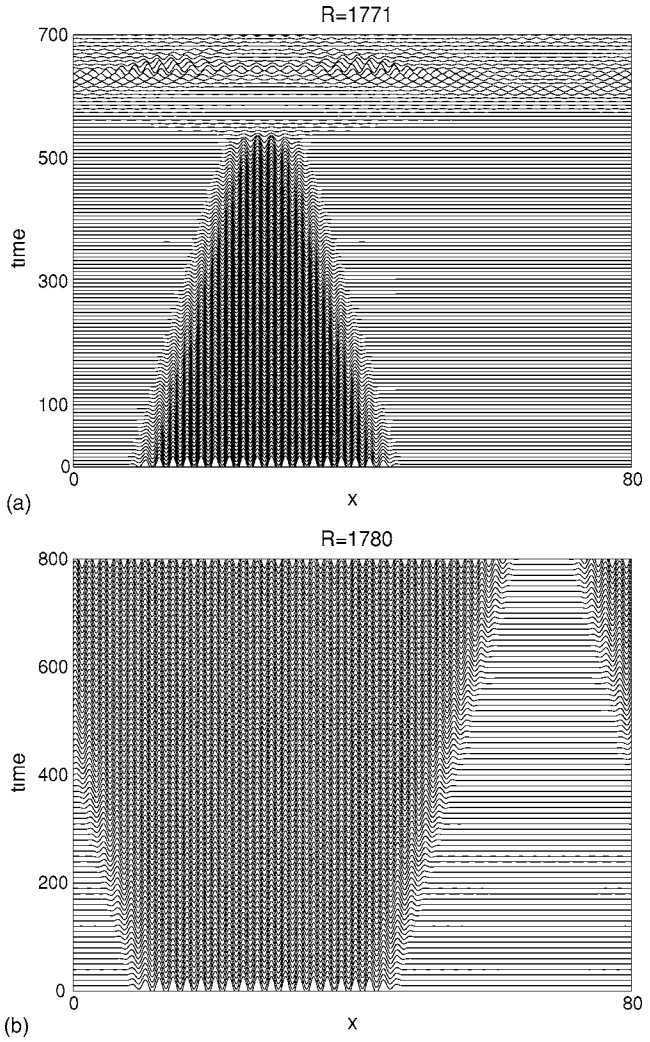

FIG. 11. Space-time plots of midplane temperature showing (a) the destruction of a stationary localized state by the progressive erosion of pairs of rolls for $R=1771$, and (b) the transition from a stationary localized state to spatially uniform stationary convection due to the unpinning of the fronts for $R=1780$.

and some differences in the upper part of the branches are expected to occur.

Although we have not computed the stability of the convectons along the branches, the stable convectons we have found using the time evolution code lie on portions of the branch between a left-turning point and the next right-turning point going up the snake. A detailed discussion of the properties of the convectons in water-ethanol mixtures as well as theoretical considerations about their existence, are discussed in a different work [42].

IV. CONCLUSIONS

In this paper, we have presented results for direct numerical simulations of convection in binary fluids in large-aspect-ratio containers. The periodic boundary conditions we have considered in the horizontal direction are suitable for modeling the annular cells frequently used in experiments. We have focused on binary mixtures with negative values of the separation ratio S, for which the primary bifurcation is subcritical and oscillatory, and with weak Soret coupling (S close to zero), so that nonlinear dispersion is important. For this type of mixture, complex time-dependent small-amplitude states and chaotic states, called dispersive chaos, arise near the onset of convection. Our numerical study using the full convection equations completes the previous works on such states: on one hand, the experimental works, performed on annular cells [3–5] and on rectangular cells [6], and on the other, the numerical works, in which CGLE models were considered [3,6,22].

In general terms, our numerical simulations agree with experimental observations, but there are also some discrepancies, mainly concerning (i) the frequency and shape of the bursts of convection amplitude observed before the dispersive chaos regime is reached and (ii) the localized stationary states, which were not observed in experiments unless surrounding waves were present.

First, as in experiments, we obtain that for slightly supercritical values of the control parameter the system can remain in small-amplitude states instead of making a transition to the stable spatially uniform fully nonlinear steady state. While unidirectional small-amplitude wave train states always turn out to be unstable, we have found persistent states formed by wave trains traveling in opposite directions.

Second, we observe numerically that the previous weakly nonlinear states are preceded by one or two bursts of convection amplitude. However, in the experimental observations reported in [3], the initial large amplitude burst is followed by a series of smaller-amplitude double-humped bursts that repeat aperiodically before the counterpropagating regime is reached. Unlike in these observations, we only obtain one or two of these bursts at the beginning of our simulations, and we never observe the repetition of the bursts. We think that the nature of the bursts we obtain is similar to that of the first large-amplitude burst observed in the experimental runs. The nonlinear frequency renormalization after the increase of the control parameter provokes the initial nearly uniform TW to grow to a very large amplitude, but the mutual reinforcement of amplitude and wave number spatial gradients would cause the collapse, after which the system ends up in a very small-amplitude state. Once in this weakly nonlinear regime, and provided that we do not increase the control parameter, subsequent bursts are much more rarely triggered than in experiments. This can be explained by the absence in our numerical simulations of the nonuniformities that might be present in any experimental setup.

Finally, with the computation of the snaking branches of localized stationary states we have provided the key piece that was missing to understand completely the extensive experimental observations in [3]. Unlike the weakly nonlinear states, the highly nonlinear bursts of amplitude and the dispersive chaos regime, the localized stationary states sustained by waves they report are not related to nonlinear dispersion, since they can be found in ^{3}He-^{4}He mixtures, which have a strong negative Soret coupling [2]. For the water-ethanol mixture we are considering, the narrow range of Rayleigh numbers for which these branches of steady local-

ized convection exist overlaps slightly the region of existence of the dispersive chaos regime, making transitions between such different regimes possible. We forecast that it should be possible to obtain experimentally stationary localized states of arbitrary length, although not reported in [3].

ACKNOWLEDGMENTS

We acknowledge stimulating discussions with E. Knobloch. This work has been supported by the DGICYT under Grant No. BFM2003-00657.

[1] M. C. Cross and P. C. Hohenberg, Rev. Mod. Phys. **65**, 851 (1993).
[2] O. Batiste and E. Knobloch, Phys. Rev. Lett. **95**, 244501 (2005).
[3] P. Kolodner, S. Slimani, N. Aubry, and R. Lima, Physica D **85**, 165 (1995).
[4] P. Kolodner, J. A. Glazier, and H. Williams, Phys. Rev. Lett. **65**, 1579 (1990).
[5] J. A. Glazier, P. Kolodner, and H. Williams, J. Stat. Phys. **64**, 945 (1991).
[6] E. Kaplan, E. Kuznetsov, and V. Steinberg, Phys. Rev. E **50**, 3712 (1994).
[7] P. Kolodner, C. M. Surko, and H. Williams, Physica D **37**, 319 (1989).
[8] V. Steinberg, J. Fineberg, E. Moses, and I. Rehberg, Physica D **37**, 359 (1989).
[9] A. C. Newell, *Nonlinear Wave Motion*, Lectures in Applied Mathematics Vol. 15 (AMS, Providence, RI, 1974).
[10] W. Schöpf and W. Zimmermann, Europhys. Lett. **8**, 41 (1989).
[11] W. Schöpf and W. Zimmermann, Phys. Rev. E **47**, 1739 (1993).
[12] P. Coullet, S. Fauve, and E. Tirapegui, J. Phys. (France) Lett. **46**, 787 (1985).
[13] M. C. Cross, Phys. Rev. A **38**, 3593 (1988).
[14] H. U. Voss, P. Kolodner, M. Abel, and J. Kurths, Phys. Rev. Lett. **83**, 3422 (1999).
[15] W. Barten, M. Lücke, and M. Kamps, Phys. Rev. Lett. **66**, 2621 (1991).
[16] M. Lücke, W. Barten, and M. Kamps, Physica D **61**, 183 (1992).
[17] H. Riecke, Phys. Rev. Lett. **68**, 301 (1992).
[18] H. Riecke, Physica D **61**, 253 (1992).
[19] H. Herrero and H. Riecke, Physica D **85**, 79 (1995).
[20] H. Riecke and W. J. Rappel, Phys. Rev. Lett. **75**, 4035 (1995).
[21] H. Riecke, Physica D **92**, 69 (1996).
[22] C. S. Bretherton and E. A. Spiegel, Phys. Lett. **96A**, 152 (1983).
[23] W. Schöpf and L. Kramer, Phys. Rev. Lett. **66**, 2316 (1991).
[24] I. S. Aranson and L. Kramer, Rev. Mod. Phys. **74**, 99 (2002).
[25] P. Kolodner, G. Flätgen, and I. G. Kevrekidis, Phys. Rev. Lett. **83**, 730 (1999).
[26] P. Kolodner and G. Flätgen, Phys. Rev. E **61**, 2519 (2000).
[27] St. Hollinger, P. Büchel, and M. Lücke, Phys. Rev. Lett. **78**, 235 (1997).
[28] W. Barten, M. Lücke, M. Kamps, and R. Schmitz, Phys. Rev. E **51**, 5636 (1995).
[29] M. Lücke, W. Barten, P. Büchel, C. Fütterer, St. Hollinger, and Ch. Jung, in *Evolution of Structures in Dissipative Continous Systems*, edited by F. H. Busse and S. C. Müller (Springer, Berlin, 1998), p. 127.
[30] W. Barten, M. Lücke, M. Kamps, and R. Schmitz, Phys. Rev. E **51**, 5662 (1995).
[31] D. Jung and M. Lücke, Phys. Rev. Lett. **89**, 054502 (2002).
[32] D. Jung and M. Lücke, Phys. Rev. E **72**, 026307 (2005).
[33] O. Batiste, M. Net, I. Mercader, and E. Knobloch, Phys. Rev. Lett. **86**, 2309 (2001).
[34] I. Mercader, A. Alonso, and O. Batiste, Eur. Phys. J. E **15**, 331 (2004).
[35] A. Alonso, O. Batiste, and I. Mercader, J. Phys.: Conf. Ser. **14**, 180 (2005).
[36] A. Alonso and O. Batiste, Theor. Comput. Fluid Dyn. **18**, 239 (2004).
[37] G. E. Karniadakis, M. Israeli, and S. A. Orszag, J. Comput. Phys. **97**, 414 (1991).
[38] S. Zhao and M. J. Yedlin, J. Comput. Phys. **113**, 215 (1994).
[39] C. K. Mamun and L. Tuckerman, Phys. Fluids **7**, 80 (1995).
[40] I. Mercader, O. Batiste, and A. Alonso, Int. J. Numer. Methods Fluids **52**, 707 (2006).
[41] J. Burke and E. Knobloch, Phys. Rev. E **73**, 056211 (2006).
[42] O. Batiste, E. Knobloch, A. Alonso, and I. Mercader, J. Fluid Mech. **560**, 149 (2006).